AUT Journal of Electrical Engineering

AUT J. Elec. Eng., 57(3) (2025) 499-514
DOI: 10.22060/eej.2025.24045.5648

Optimal Design of Low-Cost Coaxial Magnetic Gear with Hybrid Permanent Magnets

Seyed Ahmadreza Afsari*, Mostafa Madanchi Zaj, Ali Asadollahi, Mojtaba Malakooti Khaledi

Faculty of Electrical and Computer Engineering, University of Kashan, Kashan, Iran.

ABSTRACT: Magnetic gears transfer power similarly to mechanical gears between exclusive speeds and torques; however, magnetic gears' contactless structures offer inherent performance advantages over mechanical gears. Nevertheless, the cost of fluctuation and the restricted availability of rare-earth permanent magnets have hindered the broader adoption of magnetic gear technology. To minimize the consumption of the rare-earth permanent magnet material, this paper proposes a less-rare-earth magnetic gear layout wherein the inner rotor uses spoke-type magnet slots filled with each rare-earth and ferrite permanent magnets to form a hybrid permanent magnet excitation. This rotor topology employs an additional asymmetric flux barrier in each pole for torque density enhancement and cogging torque suppression. For a more comprehensive study, the permanent magnet's geometry was modeled using a trapezoidal shape. The influence of permanent magnets and barriers geometry parameters on air gap flux density was analyzed. The torque performance of the less-rare-earth magnetic gear was analyzed through 2-D and 3-D finite element analysis and compared with conventional spoke-type and flat-type interior permanent magnet rotors.

Review History:
Received: Apr. 07, 2025
Revised: Jun. 04, 2025
Accepted: Jun. 26, 2025
Available Online: Oct. 20, 2025

Keywords:
Ferrite PM
Rare-Earth PM
Hybrid Magnet
Magnetic Gear
FEM
Torque Density
Cogging Torque

1- Introduction

Magnetic gears (MGs) have emerged as a promising alternative to traditional mechanical gears, addressing many of the inherent limitations, such as mechanical wear, noise, vibrations, the necessity for lubrication, and lack of overload protection [1, 2]. Unlike mechanical counterparts that rely on direct tooth engagement, MGs utilize modulated magnetic fields to transfer torque without physical contact. This non-contact nature leads to enhanced durability, reduced maintenance requirements, inherent overload protection, and acoustic noise reduction, while also enabling physical isolation between input and output shafts [3].

With ongoing advancements in MG structures, the maximum torque density of rare-earth permanent magnet (PM)-based MGs has exceeded 250 kNm/m³ [4], highlighting their competitive potential in high-demand applications such as wind energy systems [5, 6], marine propulsion [7], and electric or hybrid vehicles [8-10].

MG-integrated motors have attracted attention due to their compact size, high torque density, and silent operation. Various studies have proposed improved designs: from magnetic-geared bearings less high-speed rotor integration [11] and cost-optimized radial flux structures [2], to novel MG integrated switched reluctance motor topologies [12] and a continuously variable magnetic geared dual stator motor [13]. These innovations have enhanced torque performance, modularity, and robustness, while also facilitating non-contact tool-changing mechanisms and efficient design methodologies using advanced simulation techniques.

To enhance torque density further, many researchers have employed rare-earth PMs like NdFeB [14-16]. However, their high cost and supply volatility motivate the exploration of alternatives. Accordingly, studies have investigated reducing rare-earth content by incorporating ferrite magnets or developing hybrid configurations that maintain performance while decreasing material dependency [17, 18]. For instance, flux-focusing ferrite-based motors [19] and hybrid magnet machines offer cost benefits and structural simplicity, though they often require sophisticated design strategies to achieve torque densities comparable to rare-earth systems. Due to the low torque density of ferrite machines, particular design techniques are inevitable to be comparable with rare-earth machines [20]. Hence, hybrid PM topologies, as an effective solution, have been strongly considered in cases where the co-excitation sources are applied with NdFeB PM and ferrite PM materials [21-23]. The optimal geometry and arrangement of different types of PMs influence the electromagnetic performances of machines significantly. [24] proposes a PM-assisted synchronous reluctance motor with a ferrite magnet without rare-earth PMs, considering

*Corresponding author's email: afsari@kashanu.ac.ir

productivity. Results illustrate that the suggested model has the same power density and equivalent efficiency as rare-earth PM synchronous motors for hybrid electric vehicles. [25] introduces different rotor configurations with a combination of ferrite and rare-earth PMs to reduce costs. The results show that this combination can compete with conventional rare-earth and spoke-type configurations. This originates from a strong funnel effect for the magnetic flux to the extent that the relatively weak flux density from the ferrite magnets is amplified to be comparable with conventional rare-earth PMs; that is, to the point of steel saturation.

Particularly, spoke-type interior permanent magnet (IPM) motors have been a focus due to their potential for performance improvement through novel barrier shapes and asymmetric configurations [26, 27]. These designs have demonstrated significant improvements in torque ripple mitigation and flux control. In [28, 29], a novel asymmetric IPM rotor topology that has a mixed V-shape and spoke-type PM configuration is designated with asymmetric flux barriers to show torque enhancement and cogging torque mitigation.

As shown in Fig. 1, radial flux MGs with three different rotors, two of which have PMs, face challenges related to PM placement and cost. This issue is particularly more severe in the case of an inner rotor with a higher rotational speed. Different structures of inner rotor PM placement are reported, including: surface-mounted PM [30], flat-type interior PM (IPM) [31], spoke-type IPM [32], and V-type IPM [33]. Since the inner rotor has fewer PMs than the outer PM rotor, it will be more appropriate and possible to design a hybrid PM structure on it.

In this context, the proposed work focuses on the design and optimization of a hybrid-excitation IPM rotor featuring a parallel trapezoidal spoke-type arrangement of rare-earth and ferrite PMs, augmented with asymmetric flux barriers. The objective is to achieve high torque density, reduced cogging torque, and minimized magnet volume and cost, all within a compact MG structure suitable for high-speed operation.

In this article, section 2 describes the principle of operations, rotor topologies of the proposed MG, conventional MG, and the optimization parameters. The influence of the flux barrier and hybrid PM configuration on the performance of the proposed MG is investigated in Section 3. Section 4 provides the conclusion.

2- Configuration of MG

2- 1- Principle of Operation

A conventional (MG) typically consists of an inner rotor and an outer rotor, both embedded with permanent magnets (PMs), and a stationary ferromagnetic rotor located between them. The magnetic fields generated by the PMs are modulated through the ferromagnetic pole pieces of the intermediate rotor (referred to as modulators), which induce space harmonics that facilitate torque transmission between the inner and outer rotors [34, 35]. This torque transfer occurs due to the interaction of specific harmonic orders, depending on the configuration of the magnetic poles and modulation structure. The process creates a gear-like effect without any physical contact, offering advantages such as reduced mechanical wear and inherent overload protection. Based on Fourier analysis of the magnetic flux density distribution, the rotational speed of the space harmonics can be expressed as a function of their order and the modulation index. Using the Fourier series of flux density distribution, originating from PMs and modulated by modulators, reveals the rotational speed of different harmonics as [36]:

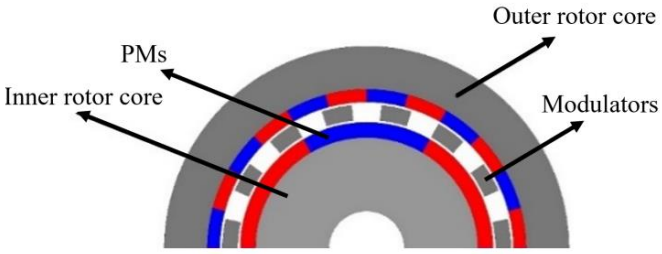

Fig. 1. Schematic of MG

$$\omega_{m,k} = \frac{mp}{kn_s + mp}\omega_r + \frac{kn_s}{kn_s + mp}\omega_s \quad (1)$$

where m is the order of the space harmonic components, and k is the order of the space harmonic components due to the introduction of the pole pieces. The combination of m =1 and k= -1 leads to a coupling of the highest harmonic magnitude with opposite rotor, and consequently, maximum torque transmission can be achieved. Hence, the relationship between the outer rotor pole pair p_o, the inner rotor pole pair p_i, and the modulators n_s, can be stated as:

$$p_o = |p_i - n_s| \quad (2)$$

The gear ratio of a magnetic gear varies depending on which rotor is held stationary. There are three main operating modes: (a) the outer rotor is fixed, (b) the modulator is fixed, and (c) the inner rotor is fixed. Each mode affects not only the torque and speed ratios but also the direction of shaft rotation.

The gear ratio when the outer rotor is held stationary (ω_r = 0), can be given by (Fig. 2-a):

$$G = \frac{-ns}{p_o - n_s} = \frac{n_s}{p_i} \quad (3)$$

The gear ratio when the modulators are held stationary (ω_s = 0), can be given by (Fig. 2-b):

$$G = \frac{p_i - n_s}{p_i} = -\frac{p_o}{p_i} \quad (4)$$

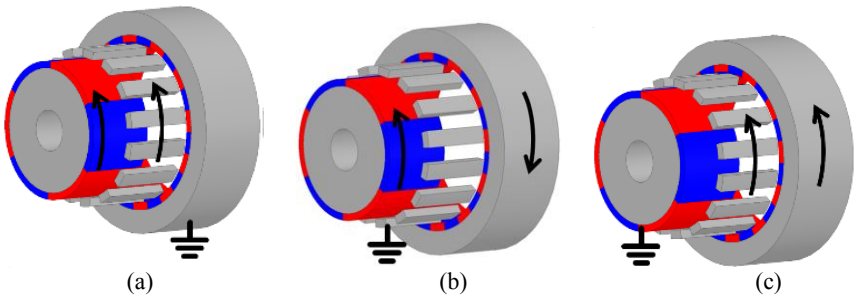

Fig. 2. Different operating modes of the magnetic gear and how the input and output rotors rotate (a) an outer rotor fixed, (b) modulator segments (pole pieces) fixed, and (c) the inner rotor fixed

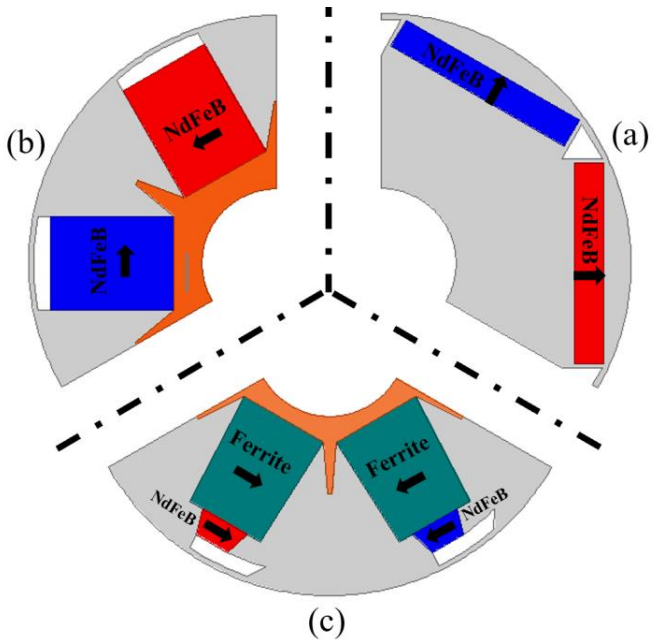

Fig. 3. Different inner rotor topologies of CMG (a): a conventional interior flat-type IPM rotor (b): a conventional spoke-type rotor and (c): a proposed asymmetric hybrid PM rotor.

When the inner rotor is kept stationary, the gear ratio can be given by (Fig. 2-c):

$$G = \frac{-n_s}{p_i - n_s} = \frac{-n_s}{p_o} \tag{5}$$

In this study, the outer rotor is kept stationary, and the inner rotor and the middle rotor act as high and low speed rotors, respectively.

2- 2- Proposed Design

To address the limitations of classical MG structures, especially the low mechanical strength of surface-mounted PMs at high rotational speeds, interior permanent magnet (IPM) configurations become essential. This is particularly critical for the high-speed inner rotor, where centrifugal forces can lead to magnet displacement or damage. In coaxial MGs using IPM configurations, the placement and geometry of PMs within the rotor core significantly affect the magnetic field distribution in the air gap. Considering the cost fluctuations and supply instability of rare-earth PMs, this study introduces a hybrid excitation approach. The proposed structure combines rare-earth (NdFeB) and non-rare-earth (ferrite) PMs arranged in a parallel spoke-type layout with asymmetric flux barriers. This configuration is designed to reduce material costs while maintaining torque performance (Fig. 3).

Fig. 3-a shows the structure of an interior flat-type magnet. In this structure, due to the limitations of the external environment of the rotor, the dimensions of the magnets are limited, and as a result, the possibility of improving the magnetic motive force will be limited. In addition, mechanical considerations in the intermediate bridges will be important due to centrifugal forces. Fig. 3-b shows a spoke-

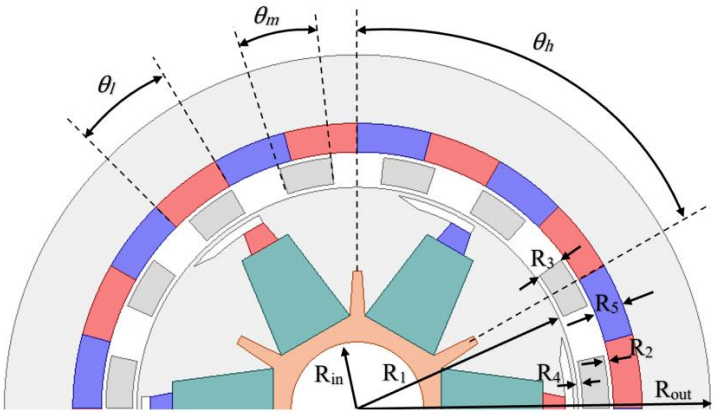

(a)

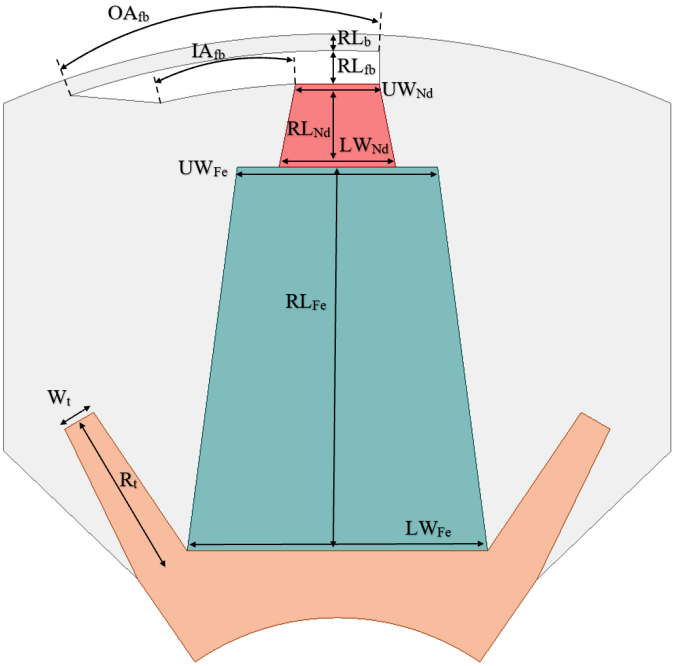

(b)

Fig. 4. (a) Proposed Inner Rotor of IPM type CMG (b) Key design variables and their geometric definitions for inner high-speed rotor

type structure with tangential magnetization. In this structure, there is a possibility of flux leakage and flux saturation due to flux concentration and interference in the inner radii. Although it is possible to change the dimensions of the magnet in this structure further, the price will also be high due to the high price of rare-earth magnets and their large volume. In Fig. 3-c, a combination of two types of magnets is used to effectively reduce the cost, and due to the larger dimensions of the ferrite type, this magnet is used in the inner radii. The trapezoidal structure of the magnets (in order to have a different magnetic motive force proportional to the reluctance of the core path) is one of the challenges of this structure, and by combining different sizes of the magnet, the desired dimensions can be achieved to some extent.

In this paper, according to the design requirements, a hybrid PM radial flux MG is presented and optimally designed. Fig. 4-a; shows the structure of the hybrid IPM rotor of MG, while design parameters are shown in Fig. 4-b. A rare-earth PM material reduction inevitably leads to magneto-motive force reduction of the PMs, which will degrade output performance. By introducing ferrite as a complementary excitation source, the output torque can be modified. The inordinate use of ferrite, PM may result in seizing the limited inner rotor space and weakening the mechanical strength of the rotor.

As illustrated in Fig. 4, the configuration ensures effective space utilization, improved magnet shaping capability, and

reduced cogging torque through the use of asymmetric flux barriers. To compare the proposed design with conventional MG topologies, certain design constraints are maintained across all models. These include identical rotor dimensions, the same number of pole pairs, and consistent axial and air gap lengths. This uniformity ensures a fair evaluation of performance improvements. The gear ratio in the proposed configuration, where the outer rotor is fixed and the inner rotor operates at high speed, is defined as 15:3 = 5. The design seeks to match or surpass the torque output of the baseline MG while minimizing the use and cost of rare-earth materials [37, 38]. The asymmetric shape of the flux barriers not only contributes to magnetic field shaping but also plays a crucial role in mitigating cogging torque. A set of geometric variables is introduced in Table 1 to define the structure within a finite element method (FEM) framework. These variables are subject to optimization to achieve the desired magnetic and mechanical performance.

2- 3- Optimization

In this study, a genetic algorithm (GA) integrated with FEM simulations is employed to optimize the geometry of the proposed MG. The objective is to achieve an optimal balance between high torque output, low cogging torque, and minimal PM usage, especially considering the cost difference between rare-earth and ferrite magnets. GA, as an evolutionary algorithm inspired by natural selection, iteratively searches for optimal solutions by performing operations such as reproduction, crossover, and mutation. The optimization process begins with a population of 100 candidate designs and proceeds for up to 2000 generations. Crossover and mutation probabilities are set at 0.7 and 0.05, respectively. The optimization framework is built within a parametric FEM-GA coupled model using Maxwell software. A set of geometric variables defines the structure of the inner rotor, including the shapes and positions of magnets and flux barriers. These variables influence magnetic flux paths, reluctance, and mechanical stability, thereby affecting key performance metrics. The flowchart of the FEM-GA coupled method is shown in Fig. 5. The Maxwell package is used to build the parameterized FE model of the proposed MG [24].

The objective function (*O.F.*) used in the optimization simultaneously targets multiple design goals: maximizing average torque, minimizing cogging torque, and reducing the volumes of ferrite and rare-earth magnets. Given the significant cost disparity—rare-earth magnets are assumed to be 15 times more expensive than ferrite magnets—the *O.F.* prioritizes efficiency per unit cost and volume. Throughout the optimization process, each design candidate is evaluated using FEM simulations to ensure electromagnetic performance is accurately assessed. The GA then selects and evolves the most promising solutions toward achieving an optimal trade-off among torque performance, magnet volume, and cogging minimization. The GA was coupled with a finite element analysis (FEA) framework to optimize the structural parameters of the proposed magnetic gear. For this purpose, an *O.F.* has been introduced to maximize it. The introduced flux barrier can provide an asymmetric and desirable distribution of the field. The dimensions of the magnets, while affecting the volume of the magnetic material and consequently its price, change the magnetic motive force and reluctance of the path to provide the best state for optimizing the objective function. The optimization is based on the following *O.F.*:

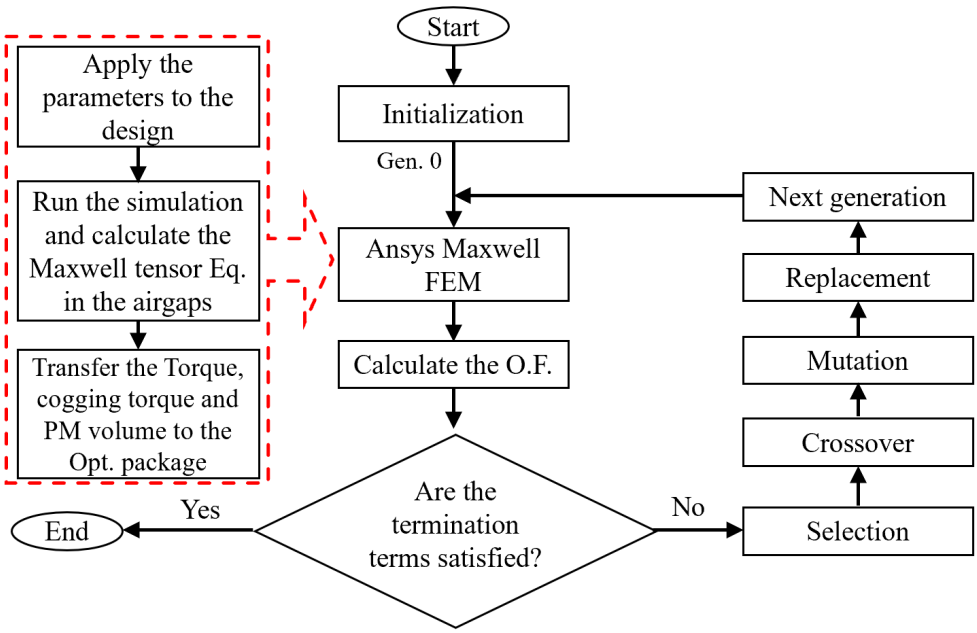

Fig. 5. The overall flowchart of the optimization procedure.

$$O.F = \frac{T_{avg(kN.m)}}{T_{cogging(\%)} \times (V_{Fe(m^3)} + 15 \times V_{Nd(m^3)})} \quad (6)$$

Average torque (T_{avg}), cogging torque percentage ($T_{Cogging}$) of the middle low-speed rotor, the volume of ferrite (V_{Fe}), and the rare-earth (V_{Nd}) PMs of the inner rotor are considered as the objectives of optimization.

The lowest price of PM, according to the ratio of price coefficients, is considered. Given the difference in the prices of NdFeB and ferrite PMs, the *O.F.* will be specified in order to get the highest efficiency from the specific volume of PMs. It should be noted that the price per volume unit of the rare-earth PMs is considered up to 15 times that of ferrite PMs, in this paper [38]. The goal of the optimization is to acquire the highest level of *O.F.* This multi-objective optimization strategy ensures that the proposed MG structure can deliver improved performance with reduced dependence on costly magnetic materials.

3- Simulation Results

The optimization process converged after 1043 iterations (Fig. 6), producing an optimal design configuration for the proposed MG. The final design parameters and corresponding performance metrics are detailed in Tables 2 and 3.

To evaluate the magnetic field distribution and torque characteristics, both 2D and 3D finite element models of the optimized MG are developed. As shown in Figs 7 and 8, the static torque of the high-speed inner rotor in the 2D model reached 7.7 Nm, while in the more accurate 3D model, it was measured at 6.139 Nm. The low-speed modulator rotor exhibited a maximum torque of 39.31 Nm and 30.59 Nm in the 2D and 3D simulations, respectively. The observed reduction of approximately 22% in the 3D results reflects the consideration of effects such as flux leakage and end effects, which are typically ignored in 2D models. In the 2-D model of the coaxial MG, the effects of factors such as saturation and leakage flux (especially the end effect) are ignored, but in the 3-D model, the effects of all these factors are considered in the torque calculation; Therefore, the reduction of the

Table 1. Design parameters of hybrid PM MG.

Predetermined parameters	***Value***
Number of high-speed rotor pole pairs (p_i)	*3*
Number of low-speed rotor pole pairs (p_o)	*12*
Number of ferromagnetic pole pieces – M6 (n_s)	*15*
Inner radius of inner rotor – M43 (R_{in})	*15 mm*
Outer radius of inner rotor – M43 (R_1)	*50 mm*
Radial length of Each air gap (R_2, R_4)	*1mm*
Radial length of ferromagnetic pole pieces (R_3)	*6 mm*
Radial length of outer rotor PMs (R_5)	*5 mm*
Effective Radial thickness of outer core – M43	*17 mm*
Outer radius of outer rotor – M43 (R_{out})	*80 mm*
Total length of MG	*50 mm*
Slot opening of ferromagnetic pole-pieces (θ_m)	*12 degrees*
Pole pitch angle of inner rotor (θ_h)	*60 degrees*
Pole pitch angle of outer rotor (θ_l)	*15 degrees*
Optimization parameters	***Boundary***
Outer arc of flux barrier (OA_{fb})	*16-25 degrees*
Inner arc of flux barrier (IA_{fb})	*4-14 degrees*
Radial length of bridge (RL_b)	*1-2 mm*
Radial length of flux barrier (RL_{fb})	*2-3.5 mm*
Upper width of NdFeB (UW_{Nd})	*4-13 mm*
Radial length of NdFeB (RL_{Nd})	*2-6 mm*
Lower width of NdFeB (LW_{Nd})	*4-13 mm*
Upper width of Ferrite (UW_{Fe})	*7-22 mm*
Radial length of Ferrite (RL_{Fe})	*15-23 mm*
Lower width of Ferrite (LW_{Fe})	*7-18 mm*
Tooth width of holder (W_t)	*1-5 mm*
Radial length of holder (R_t)	*4-12 mm*

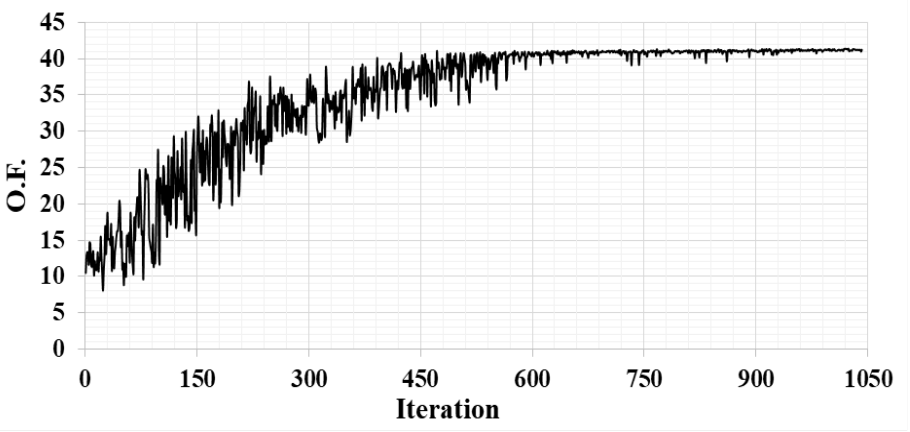

Fig. 6. Convergence curve of genetic optimization algorithm.

Table 2. Optimization results of design parameters.

Parameter	*Optimal result*
Outer arc of flux barrier (OA_{fb})	*19.9 degrees*
Inner arc of flux barrier (IA_{fb})	*7.6 degrees*
Radial length of bridge (RL_b)	*1 mm*
Radial length of flux barrier (RL_{fb})	*3 mm*
Upper width of NdFeB (UW_{Nd})	*7 mm*
Radial length of NdFeB (RL_{Nd})	*5 mm*
Lower width of NdFeB (LW_{Nd})	*9 mm*
Upper width of Ferrite (UW_{Fe})	*20 mm*
Radial length of Ferrite (RL_{Fe})	*23 mm*
Lower width of Ferrite (LW_{Fe})	*18 mm*
Tooth width of holder (W_t)	*1 mm*
Radial length of holder (R_t)	*10 mm*

Table 3. Final results of optimization performances.

Performance	*Scope*	*Value*
Volume of NdFeB (m^3)	*Min.*	$1.2*10^{-5}$
Volume of Ferrite (m^3)	*Min.*	$1.311*10^{-4}$
Average Torque (Nm)	*Max.*	*39.3103*
Cogging torque (%)	*Min.*	*3.0536*
O.F.	*Max.*	*41.381*

maximum torque value in the 3D model can be considered as a result of the mentioned factors. The cogging torque of the low-speed rotor was calculated as 3.053% in the 2D model and 3.43% in the 3D model, demonstrating the effectiveness of the asymmetric flux barriers in reducing torque ripple.

Figures 9 through 11 illustrate the optimized geometries and resulting magnetic field distributions. Specifically, the magnetic vector potential lines and flux density plots confirm that the asymmetric flux barrier structure guides the magnetic flux efficiently, enhancing torque performance and minimizing cogging.

Tables 4 and 5 compare the 2D and 3D performance metrics of three MG topologies. While conventional spoke-type structures produce higher torque, they require significantly more rare-earth PM material, leading to increased cost. In contrast, the proposed hybrid structure achieves a superior objective function value due to its improved torque-per-magnet-volume ratio and reduced reliance on costly materials. The cogging torque reduction is achieved by using the optimal shape of an asymmetric flux barrier. Maximum torque per PM volume, as an effective indicator in the useful use of PMs, is increased in the proposed hybrid PM structure. The visual comparison of the output performances of different MG topologies is shown in Fig. 12.

Temperature behaviour was also investigated, considering the distinct thermal responses of NdFeB and ferrite magnets. NdFeB magnets exhibit a shift in the B–H curve toward the second quadrant at elevated temperatures, increasing their risk of irreversible demagnetization. In contrast, ferrite magnets show improved resistance to demagnetization as temperature rises due to their positive coercivity temperature coefficient. The potential demagnetization of magnets has a

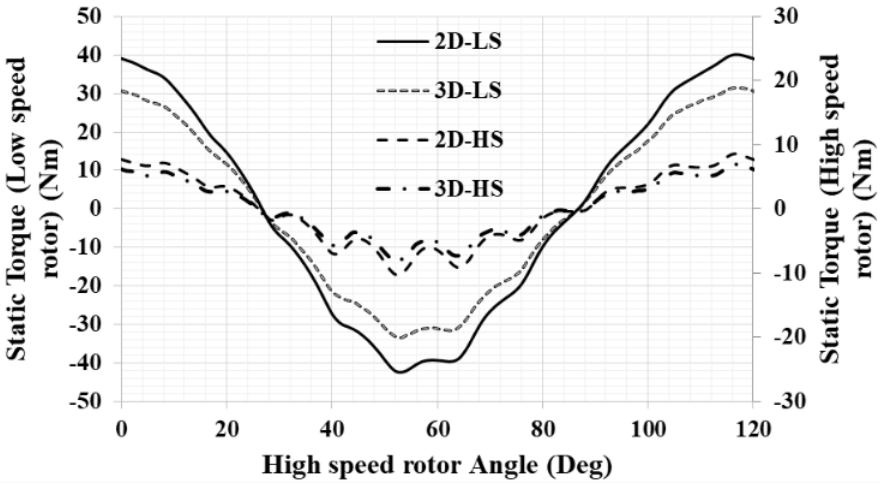

Fig. 7. The static torques waveform when the low-speed modulator is locked.

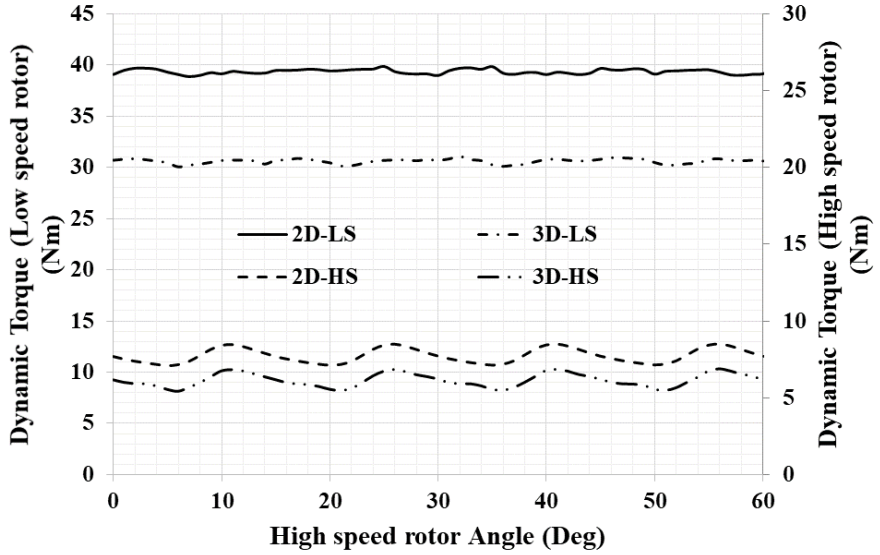

Fig. 8. Comparison of dynamic torques in optimized CMG.

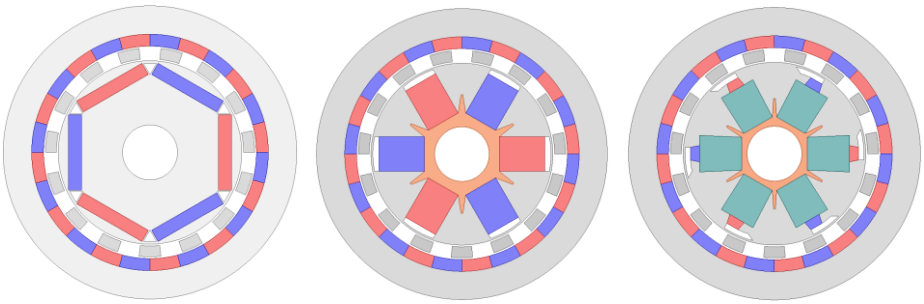

(a) (b) (c)

Fig. 9. Final optimal geometry of optimal MG (a) optimal conventional flat-type IPM rotor (b) optimal conventional spoke-type rotor, and (c) optimal proposed asymmetric hybrid PM rotor.

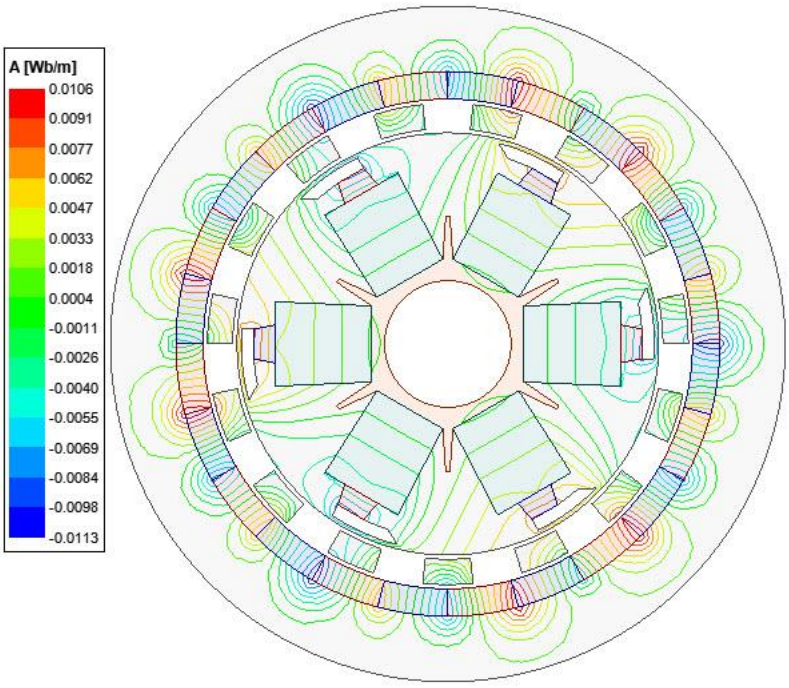

Fig. 10. 2-D cross-section view of magnetic vector potential lines distribution.

Table 4. Comparison of optimal results of different rotor topologies in 2-D designs.

Performance	*2-D results*		
	IPM	***Spoke-type***	***Proposed***
Torque $_{LS}$ (Nm)	*35*	*114.25*	*39.31*
Torque $_{HS}$ (Nm)	*7*	*22.51*	*7.74*
Torque ripple $_{LS}$ (%)	*8*	*3.21*	*3.05*
Torque ripple $_{HS}$ (%)	*53*	*9.05*	*18*
O.F.	*4.05*	*16.62*	*41.38*
Total Volume(m^3)	$1.0053*10^{-5}$	$1.0053*10^{-5}$	$1.0053*10^{-5}$
Torque density $_{LS}$(kNm/m^3)	*34.81*	*113.64*	*39.10*
NdFeB Inner Rotor Volume (m^3)	$7.2*10^{-5}$	$14.25*10^{-5}$	$1.2*10^{-5}$
Ferrite Volume (m^3)	*0*	*0*	$13.11*10^{-5}$
Torque per PM Volume (kNm/m^3)	*32.40*	*53.45*	*126.35*

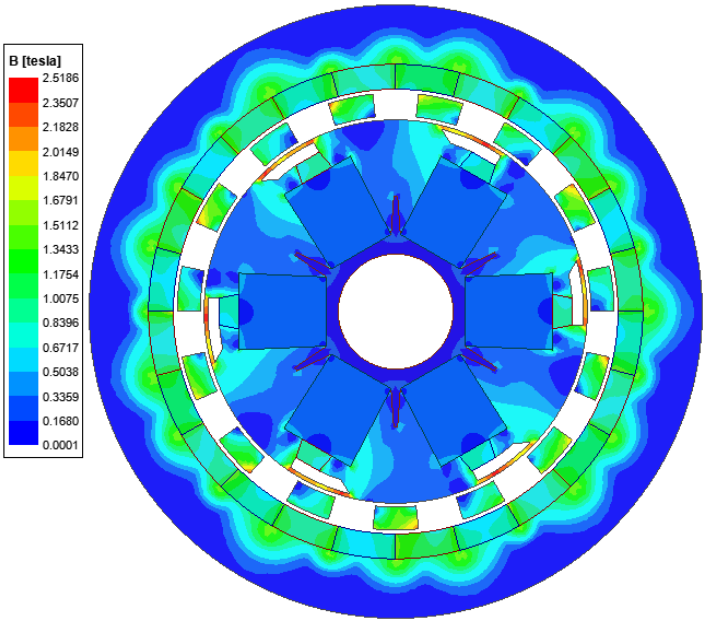

(a)

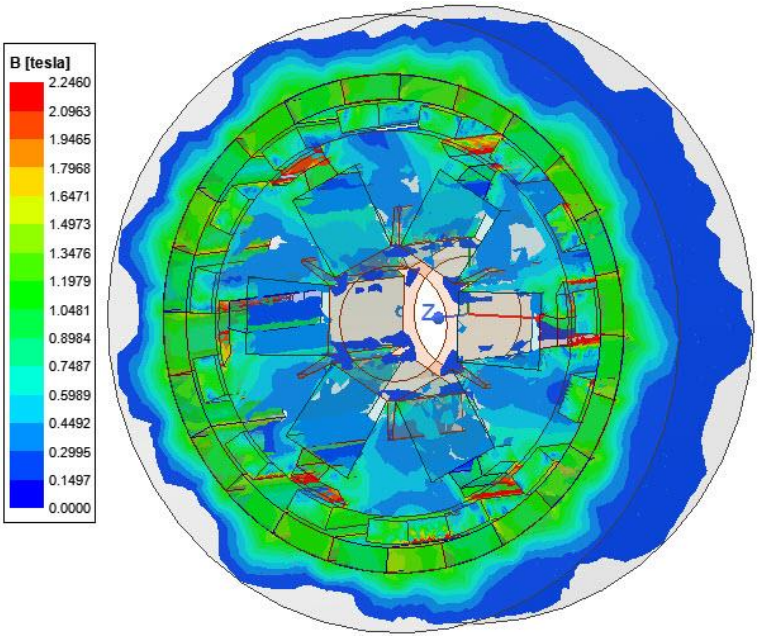

(b)

Fig. 11. Cross-sectional view of flux density distribution (a) 2-D model, and (b) 3-D model

Table 5. Comparison of optimal results of different rotor topologies in 3-D designs.

Performance	*3-D results*		
	IPM	***Spoke-type***	***Proposed***
Torque $_{LS}$ (Nm)	*29.1*	*88*	*30.59*
Torque $_{HS}$ (Nm)	*5.8*	*17.50*	*6.13*
Torque ripple $_{LS}$ (%)	*7.2*	*5.12*	*3.43*
Torque ripple $_{HS}$ (%)	*51*	*15.74*	*18.84*
O.F.	*3.7422*	*8.0365*	*28.6043*
Total Volume(m^3)	$1.0053*10^{-5}$	$1.0053*10^{-5}$	$1.0053*10^{-5}$
Torque density $_{LS}$(kNm/m^3)	*28.94*	*87.53*	*30.43*
NdFeB Inner Rotor Volume (m^3)	$7.2*10^{-5}$	$14.25*10^{-5}$	$1.2*10^{-5}$
Torque density $_{LS}$(kNm/m^3)	*28.94*	*87.53*	*30.43*
Torque per Magnet Volume (kNm/m^3)	*26.94*	*47.17*	*98.34*

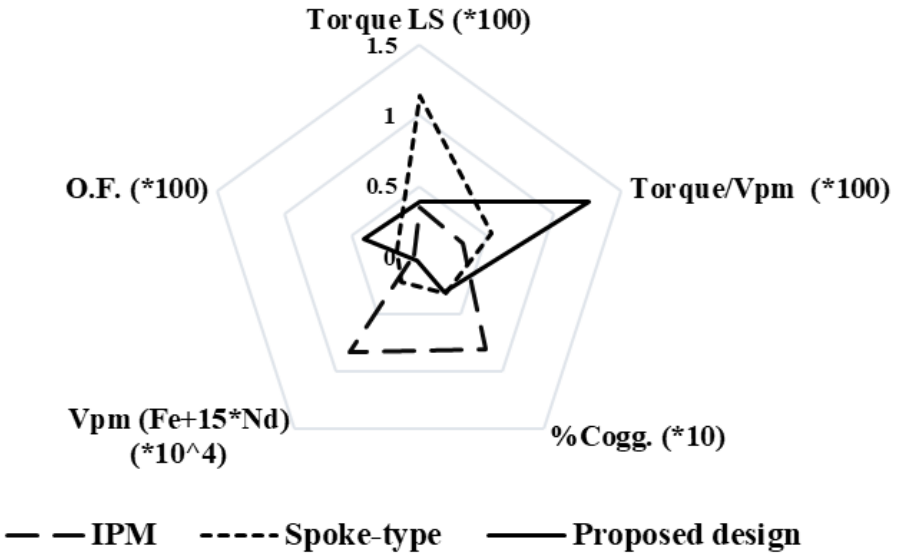

Fig. 12. Visual comparison of optimal results of different rotor topologies (2-D design).

consequential degrading effect on MG performance.

Due to the positive temperature coefficient of coercivity, ferrite PMs are more likely to get demagnetized at low-temperature conditions. The potential demagnetization of magnets has a consequential degrading effect on MG performance and, therefore, has been the subject of interest in many research works. The irreversible demagnetization occurs when the PM's flux density of the magnet becomes less than the threshold level at the knee point. Demagnetization analysis of the ferrite magnets was conducted under both no-load and full-load conditions. Results, shown in Fig. 13, indicate that the flux from adjacent NdFeB magnets reinforces the ferrite operating point, ensuring that the flux density remains above the demagnetization threshold of 0.2 T [39]. This mutual reinforcement improves the anti-demagnetization capability of the hybrid rotor.

To assess mechanical integrity, a centrifugal force analysis was performed using ANSYS R17.2. The von Mises stress distribution, shown in Figs 14 and 15, revealed that the maximum stress and total deformation distribution occur at the tips of the inner rotor bridges at a rotational speed of 16500 rpm. The stress levels remain below the yield strength

Fig. 13. Demagnetization analysis results of ferrite PM (a) No-load (zero torque transmission position) magnetic field distributions (b) Full-load (maximum torque transmission position) magnetic field distribution

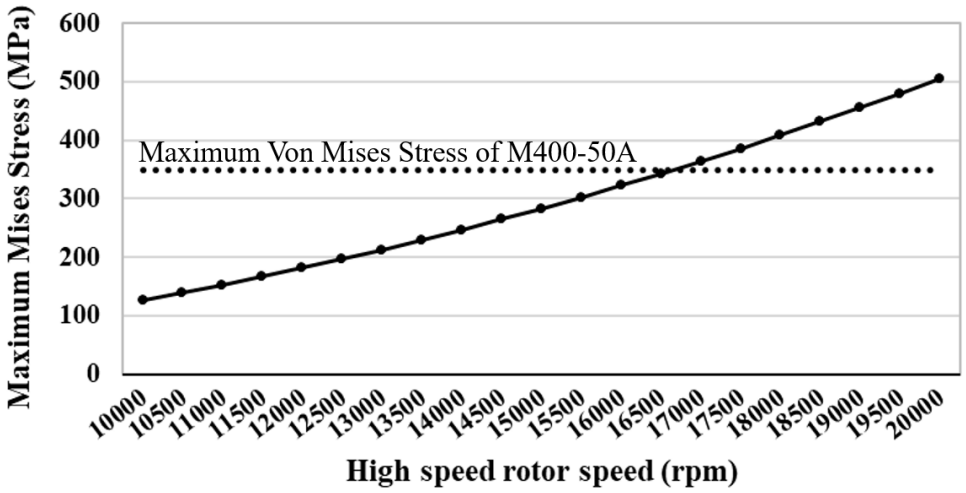

Fig. 14. Maximum von Mises stress of FB rotor according to the speed of HS rotor.

(350 MPa) of the rotor material (M400-50A), indicating acceptable structural performance at the intended operating speed.

Finally, iron loss analysis demonstrated a clear advantage of the proposed design. As shown in Fig. 16, the hybrid MG experiences 46% less iron loss compared to the conventional spoke-type MG (2.41 W vs. 4.5 W), confirming improved efficiency.

4- Conclusion

In this article, a new structure of coaxial MG based on hybrid PM was proposed. In the inner rotor of this structure, to reduce the cost and to increase the torque density, two types of magnetic material (ferrite and rare-earth PMs) with trapezoidal spoke-type structure were used. Also, in the internal rotor of the proposed coaxial MG, asymmetric flux barriers were created to control the distribution of flux density in the air gap and minimize cogging torque. The proposed structure was optimized with the aim of maximizing the torque density and minimizing the volume of the internal rotor magnetic material and cogging torque by a genetic optimization algorithm and finite element software. The optimized structure was analysed by 2-D and 3-D FEM analysis, and it was concluded that 10 and 2.5 times increase in O.F. can be extracted by the proposed hybrid PM MG compared with optimal conventional flat-type IPM and conventional spoke-type PM MGs, respectively. This improvement is accompanied by an effective increase in

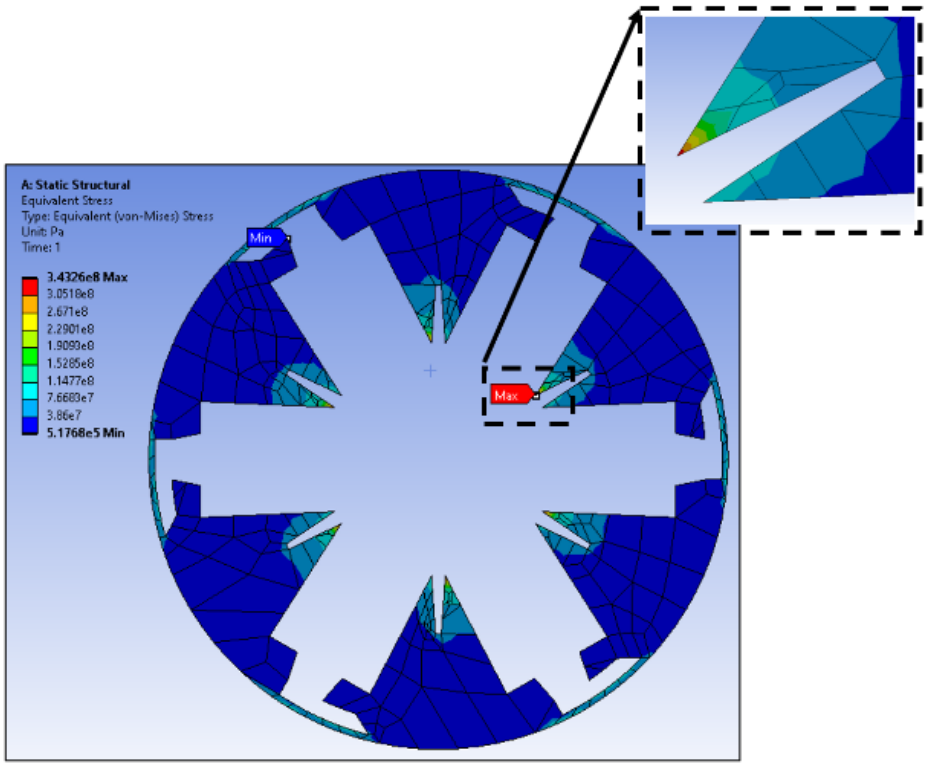

(a)

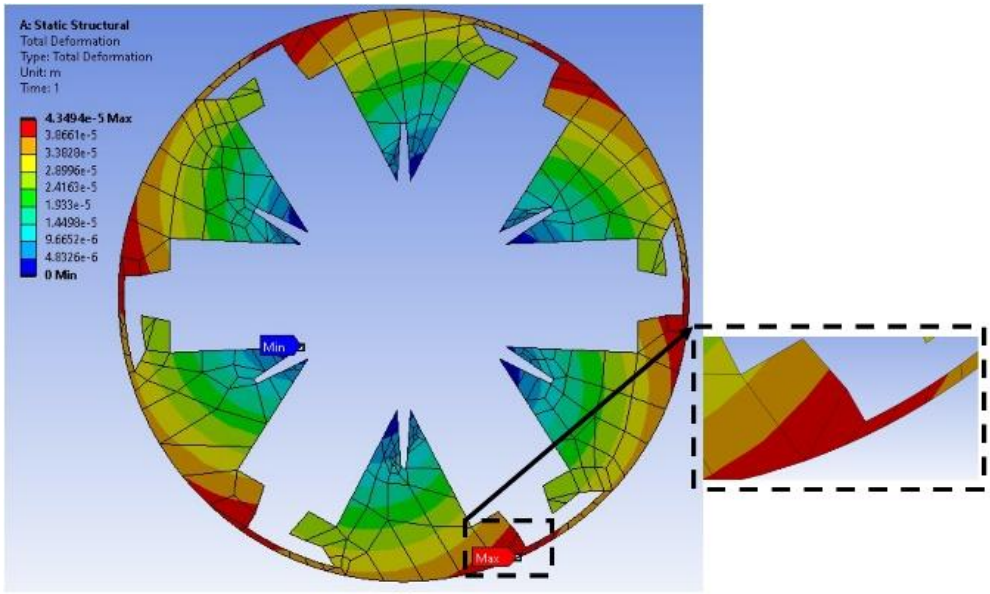

(b)

Fig. 15. Mechanical analysis of FB rotor in 12000 rpm (a) Mises stress distribution and (b) total deformation distribution

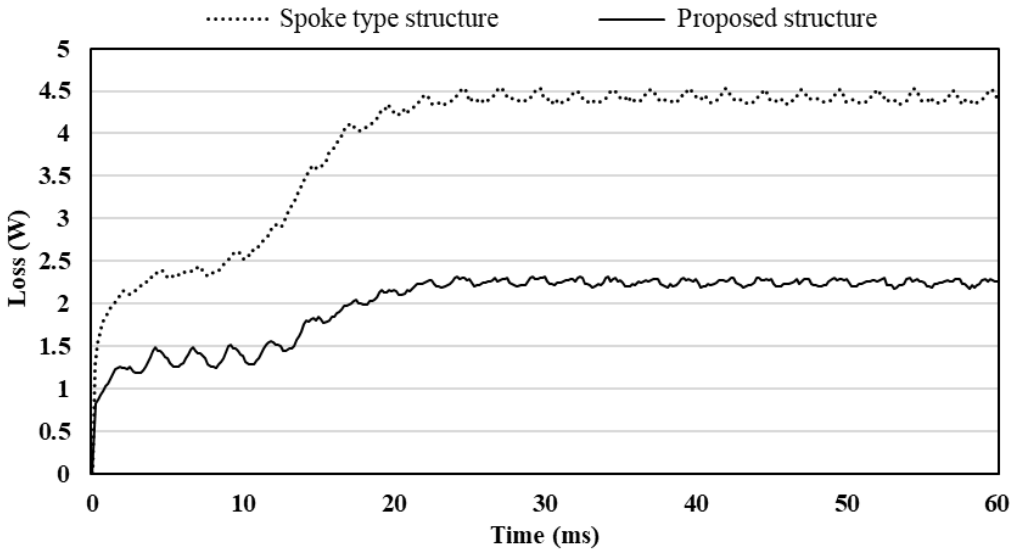

Fig. 16. The loss comparison of the optimal spoke type and proposed MG.

the torque per magnet volume of about 3.9 and 2.36 times compared with optimal conventional flat-type IPM and conventional spoke-type PM MGs, respectively. The results of the 3-D model show a reduction compared to the values of the 2-D model. This decrease in value is justified by referring to the weakness of the 2-D model in applying the end effect and ignoring the leakage flux in the third dimension; it was revealed that the 3-D model provided more accurate results than the 2-D model.

References

[1] S. Yousefnejad, H. Heidary, J.S. Ro, E. Amiri, S.E. Afjei, K. Akatsu, A Novel Structure of Magnetic-Geared Permanent Magnet Machine Based on Halbach Array, in: 2022 IEEE Kansas Power and Energy Conference (KPEC), 2022, pp. 1–6.

[2] G. Tao, B. Praslicka, S. Hasanpour, T. Simms, Z. Wibisono, M.C. Gardner, M. Johnson, E. Hankins, M. McCall, A. Roussie, S. Ortiz, W. Thiele, H.A. Toliyat, Experimental Comparison of Acoustic Characteristics for a High-Efficiency Magnetic Gearbox and a Mechanical Planetary Gearbox for Industrial HVAC Applications, IEEE Transactions on Energy Conversion, 39(1) (2024) 182–190.

[3] J.X. Shen, H.Y. Li, H. Hao, M.J. Jin, A Coaxial Magnetic Gear With Consequent-Pole Rotors, IEEE Transactions on Energy Conversion, 32(1) (2017) 267–275.

[4] X. Yin, P.D. Pfister, Y. Fang, A Novel Magnetic Gear: Toward a Higher Torque Density, IEEE Transactions on Magnetics, 51(11) (2015) 1–4.

[5] Q. Qin, B. Cai, Y. Du, Nonlinear Dynamic Characteristic Analysis Method Based on Load Angle of Two-Stage Magnetic Gearbox for Wind Turbine, IEEE Access, 11 (2023) 109038–109048.

[6] T. Sumi, A. Okazaki, K. Nakamura, T. Shinji, K. Takeda, Torque-to-Weight Ratio Improvement and Permanent Magnet Usage Reduction in Large-Scale Magnetic Gears for Wind Power Generation, in: 2024 IEEE International Magnetic Conference - Short papers (INTERMAG Short papers), 2024, pp. 1–2.

[7] N.W. Frank, H.A. Toliyat, Gearing ratios of a magnetic gear for marine applications, in: 2009 IEEE Electric Ship Technologies Symposium, 2009, pp. 477–481.

[8] L. Jing, W. Tang, T. Wang, T. Ben, R. Qu, Performance Analysis of Magnetically Geared Permanent Magnet Brushless Motor for Hybrid Electric Vehicles, IEEE Transactions on Transportation Electrification, 8(2) (2022) 2874–2883.

[9] M. Filippini, R. Torchio, P. Alotto, E. Bonisoli, L. Dimauro, M. Repetto, A New Class of Devices: Magnetic Gear Differentials for Vehicle Drivetrains, IEEE Transactions on Transportation Electrification, 9(2) (2023) 2382–2397.

[10] S. Xie, Y. Zuo, Z. Song, S. Cai, F. Shen, J. Goh, B.S. Han, C.C. Hoang, C.H.T. Lee, A Magnetic-Geared Machine With Improved Magnetic Circuit Symmetry for Hybrid Electric Vehicle Applications, IEEE Transactions on Transportation Electrification, 10(1) (2024) 2170–2182.

[11] A. Kumashiro, L. Chen, Y. Fujii, A. Chiba, W. Gruber, W. Amrhein, G. Jungmayr, Novel Reluctance-Type Magnetic-Geared Motor Integrated With High-Speed Bearingless Motor, IEEE Transactions on Industry Applications, 60(3) (2024) 3808–3819.

[12] S. Dey, B.G. Fernandes, K. Chatterjee, A High Torque Density Magnetic Geared Switched Reluctance Motor for In-wheel Applications, in: 2024 IEEE Transportation Electrification Conference and Expo (ITEC), 2024, pp. 1–6.

[13] S.K. Warsi, S. Sashidhar, A Novel Continuously Variable Magnetic Geared Dual Stator Hub-Motor for an E-Bike,

in: 2024 IEEE International Magnetic Conference - Short papers (INTERMAG Short papers), 2024, pp. 1–2.

[14] Y. Chen, W.N. Fu, S.L. Ho, H. Liu, A Quantitative Comparison Analysis of Radial-Flux, Transverse-Flux, and Axial-Flux Magnetic Gears, IEEE Transactions on Magnetics, 50(11) (2014) 1–4.

[15] X. Zhang, X. Liu, Z. Chen, A Novel Coaxial Magnetic Gear and Its Integration With Permanent-Magnet Brushless Motor, IEEE Transactions on Magnetics, 52(7) (2016) 1–4.

[16] S.A. Afsari, H. Heydari, E. Bashar, Viable Arcuate Double-sided Magnetic Gear for Competitive Torque Density Transmission Capability, Scientia Iranica, 23(3) (2016) 1251–1260.

[17] B. Sun, Z. Wang, Z. Song, G. Wang, J. Huang, Z. Zhang, X. Zhang, Research on the integrated magnetic field modulation motor, in: CSAA/IET International Conference on Aircraft Utility Systems (AUS 2022), 2022, pp. 316–321.

[18] M.A. Masoudi, S.A. Afsari, The Optimal Design and an Analysis of a Hybrid W-Shaped IPM Rotor of Coaxial Magnetic Gear, IEEE Access, 12 (2024) 81067–81074.

[19] S.I. Kim, J. Cho, S. Park, T. Park, S. Lim, Characteristics Comparison of a Conventional and Modified Spoke-Type Ferrite Magnet Motor for Traction Drives of Low-Speed Electric Vehicles, IEEE Transactions on Industry Applications, 49(6) (2013) 2516–2523.

[20] Y. Zhou, Y. Chen, J.X. Shen, Analysis and Improvement of a Hybrid Permanent-Magnet Memory Motor, IEEE Transactions on Energy Conversion, 31(3) (2016) 915–923.

[21] A.S. Al-Adsani, O. Beik, Design of a Multiphase Hybrid Permanent Magnet Generator for Series Hybrid EV, IEEE Transactions on Energy Conversion, 33(3) (2018) 1499–1507.

[22] I. Boldea, L.N. Tutelea, L. Parsa, D. Dorrell, Automotive Electric Propulsion Systems With Reduced or No Permanent Magnets: An Overview, IEEE Transactions on Industrial Electronics, 61(10) (2014) 5696–5711.

[23] Q. Chen, G. Liu, W. Zhao, M. Shao, Z. Liu, Design and Analysis of the New High-Reliability Motors With Hybrid Permanent Magnet Material, IEEE Transactions on Magnetics, 50(12) (2014) 1–10.

[24] M. Obata, S. Morimoto, M. Sanada, Y. Inoue, Performance of PMASynRM With Ferrite Magnets for EV/HEV Applications Considering Productivity, IEEE Transactions on Industry Applications, 50(4) (2014) 2427–2435.

[25] Q. Ma, A. El-Refaie, B. Lequesne, Low-Cost Interior Permanent Magnet Machine With Multiple Magnet Types, IEEE Transactions on Industry Applications, 56(2) (2020) 1452–1463.

[26] J. Li, K. Wang, A Novel Spoke-Type PM Machine Employing Asymmetric Modular Consequent-Pole Rotor, IEEE/ASME Transactions on Mechatronics, 24(5) (2019) 2182–2192.

[27] X. Ge, Z.Q. Zhu, J. Li, J. Chen, A Spoke-Type IPM Machine With Novel Alternate Airspace Barriers and Reduction of Unipolar Leakage Flux by Step-Staggered Rotor, IEEE Transactions on Industry Applications, 52(6) (2016) 4789–4797.

[28] Y. Xiao, Z.Q. Zhu, J.T. Chen, D. Wu, L.M. Gong, A Novel Asymmetric Interior Permanent Magnet Synchronous Machine, in: 2020 International Conference on Electrical Machines (ICEM), 2020, pp. 26–32.

[29] Y. Xiao, Z.Q. Zhu, G.W. Jewell, J. Chen, D. Wu, L. Gong, A Novel Spoke-Type Asymmetric Rotor Interior Permanent Magnet Machine, IEEE Transactions on Industry Applications, 57(5) (2021) 4840–4851.

[30] K. Atallah, D. Howe, A novel high-performance magnetic gear, IEEE Transactions on Magnetics, 37(4) (2001) 2844–2846.

[31] N.W. Frank, H.A. Toliyat, Analysis of the Concentric Planetary Magnetic Gear With Strengthened Stator and Interior Permanent Magnet Inner Rotor, IEEE Transactions on Industry Applications, 47(4) (2011) 1652–1660.

[32] P.O. Rasmussen, T.O. Andersen, F.T. Jorgensen, O. Nielsen, Development of a high-performance magnetic gear, IEEE Transactions on Industry Applications, 41(3) (2005) 764–770.

[33] S. Zhu, Y. Hu, C. Liu, B. Jiang, Shaping of the Air Gap in a V-Typed IPMSM for Compressed-Air System Applications, IEEE Transactions on Magnetics, 57(2) (2021) 1–5.

[34] K. Dong, H. Yu, M. Hu, Study of an Axial-Flux Modulated Superconducting Magnetic Gear, IEEE Transactions on Applied Superconductivity, 29(2) (2019) 1–5.

[35] S.A.A. Kashani, Rotor Pole Design of Radial Flux Magnetic Gear for Reduction of Flux Density Harmonics and Cogging Torque, IEEE Transactions on Applied Superconductivity, 29(8) (2019) 1–8.

[36] B. Dianati, H. Heydari, S.A. Afsari, Analytical Computation of Air-Gap Magnetic Field in a Viable Superconductive Magnetic Gear, IEEE Transactions on Applied Superconductivity, 26(6) (2016) 1–12.

[37] L. Jian, K.T. Chau, A Coaxial Magnetic Gear With Halbach Permanent-Magnet Arrays, IEEE Transactions on Energy Conversion, 25(2) (2010) 319–328.

[38] X. Zhu, W. Wu, L. Quan, Z. Xiang, W. Gu, Design and Multi-Objective Stratified Optimization of a Less-Rare-Earth Hybrid Permanent Magnets Motor With High Torque Density and Low Cost, IEEE Transactions on Energy Conversion, 34(3) (2019) 1178–1189.

[39] B. Poudel, E. Amiri, P. Rastgoufard, B. Mirafzal, Toward Less Rare-Earth Permanent Magnet in Electric Machines: A Review, IEEE Transactions on Magnetics, 57(9) (2021) 1–19.

HOW TO CITE THIS ARTICLE
S. A. R. Afsari, M. Madanchi Zaj, A. Asadollahi, M. Malakooti Khaledi, Optimal Design of Low-Cost Coaxial Magnetic Gear with Hybrid Permanent Magnets, AUT J. Elec. Eng., 57(3) (2025) 499-514.

DOI: 10.22060/eej.2025.24045.5648